

Electronic structure of TiSi_2

L. F. Mattheiss and J. C. Hensel

AT&T Bell Laboratories, Murray Hill, New Jersey 07974

(Received 23 December 1988)

The linear augmented-plane-wave method has been applied to calculate the electronic structure and properties of the orthorhombic metastable base-centered (*C49*) and equilibrium face-centered (*C54*) phases of TiSi_2 . Despite the structural differences, both polytypes exhibit similar electronic properties, including broad low-lying Si $3s$ - $3p$ bands, partially filled Ti $3d$ bands, and density-of-states minima within the $3d$ -band manifold near E_F . The high residual resistivity of *C49* films in comparison with those having the *C54* structure (~ 27 versus $0.7 \mu\Omega \text{ cm}$) is analyzed with the use of the calculated Drude plasma energy and Fermi velocity for the two polytypes. It is concluded that the comparatively short scattering length of the *C49* phase ($l_c \approx 90 \text{ \AA}$ versus $\sim 990 \text{ \AA}$ for *C54* TiSi_2) is an extrinsic property, caused primarily by the presence of heavily faulted microstructure in the *C49* films.

Transition-metal silicides are finding increasingly important applications in silicon integrated-circuit technology as Schottky barriers, Ohmic contacts, and low-resistivity interconnects. Within this family of compounds, the refractory disilicides (i.e., those containing one of the group-IVB, -VB, or -VIB elements) have attracted special attention because of their high-temperature stability and their relatively low resistivities.¹ Unlike the group-VIII disilicides CoSi_2 and NiSi_2 , which have the cubic fluorite structure, the refractory disilicides form with more complicated, low-symmetry orthorhombic (group IVB), hexagonal (group VB), and hexagonal-tetragonal (group VIB) structures.

A comprehensive survey¹ has shown that TiSi_2 has the lowest thin-film resistivity within the entire silicide family. It is rapidly becoming the material of choice in silicon-chip applications. This has led to rather extensive studies²⁻⁴ of the detailed process by which metallic Ti films that are deposited on Si substrates are converted to low-resistivity TiSi_2 films.

On the basis of their transmission-electron-microscope studies, Beyers and Sinclair² have determined that the formation of low-resistivity TiSi_2 thin films on Si substrates takes place in two stages. In the first stage, a deposited Ti film or Ti-Si mixture reacts with the Si substrate at relatively low temperatures (500 – 550°C) to form a metastable TiSi_2 phase (*C49* structure) that is heavily faulted and has a relatively high room-temperature resistivity (60 – $300 \mu\Omega \text{ cm}$). Further elevation of the temperature subsequently causes the metastable *C49* phase to transform at some point to an equilibrium TiSi_2 phase (*C54* structure) which is fault free and has a significantly lower resistivity ($\sim 15 \mu\Omega \text{ cm}$). This general picture has been confirmed by more recent x-ray-diffraction studies.^{3,4} In addition, it is now recognized that the *C49*→*C54* transition temperature depends on certain experimental factors such as film thicknesses.³

The existence of two TiSi_2 polytypes with base-centered (*C49*) and face-centered (*C54*) orthorhombic structures raises interesting questions as to whether these

pronounced resistivity differences are intrinsic or extrinsic. This has led to detailed studies⁴ of the transport properties of the two phases, including the effect of the annealing temperature on the *C49*-*C54* transition.

Because of the enormous potential of TiSi_2 in future technological applications, a comprehensive understanding of the bulk electronic properties for both the metastable (*C49*) and equilibrium (*C54*) phases is desirable. Accordingly, we have carried out electronic band-structure calculations for the *C49* and *C54* phases of TiSi_2 with the use of the linear augmented-plane-wave (LAPW) method.⁵ Although the existing experimental data on the electronic properties of TiSi_2 is quite sparse, limited at present to rather low-resolution photoemission results,⁶⁻⁸ it is anticipated that these materials will be the focus of more comprehensive experimental studies in the future.

The primitive unit cell for both the *C49* and *C54* crystal structures contains two TiSi_2 molecules. The arrangement of Ti atoms is significantly different in the two phases. The *C49* structure is characterized by (010) double layers of Ti atoms whose width ($\sim 2.8 \text{ \AA}$) is small compared to the interlayer separation ($\sim 4.1 \text{ \AA}$). In the *C54* phase, the Ti sites correspond to those of a distorted diamond-type structure with orthorhombic lattice parameters $a \approx 2b \approx c$. However, the coordination of Si atoms about the Ti sites is similar in both structures. Each Ti atom has ten near-neighbor Si atoms at distances in the range 2.6 – 2.8 \AA .

The space groups for both structures are nonsymmetrical, containing nonprimitive translations. The symmetry of the *C49* structure corresponds to the D_{2h}^{17} (*Cmcm*) space group. It involves a one-face-centered orthorhombic Bravais lattice with primitive vectors

$$\begin{aligned} \mathbf{t}_1 &= \frac{1}{2}a\hat{\mathbf{i}} + \frac{1}{2}b\hat{\mathbf{j}}, \\ \mathbf{t}_2 &= -\frac{1}{2}a\hat{\mathbf{i}} + \frac{1}{2}b\hat{\mathbf{j}}, \\ \mathbf{t}_3 &= c\hat{\mathbf{k}}. \end{aligned} \quad (1)$$

TABLE I. Lattice parameters, internal structural parameters, and atom position coordinates for the orthorhombic $C49$ and $C54$ phases of TiSi_2 (Ref. 9). The internal position parameters are listed in terms of their components. $(\alpha, \beta, \gamma) = \alpha \hat{a} + \beta \hat{b} + \gamma \hat{c}$.

	$C49$	$C54$
a (Å)	3.62	8.253
b (Å)	13.76	4.783
c (Å)	3.605	8.540
u	0.1022 ^a	0.333
v	0.7522 ^a	
w	0.4466 ^a	
Ti	$\pm(0, u, \frac{1}{4})$	$(0, 0, 0), (\frac{1}{4}, \frac{1}{4}, \frac{1}{4})$
Si	$\pm(0, v, \frac{1}{4})$ (I) $\pm(0, w, \frac{1}{4})$ (II)	$\pm(u, 0, 0)$ $(\frac{1}{4} \pm u, \frac{1}{4}, \frac{1}{4})$

^aInternal position parameters for ZrSi_2 (Ref. 9).

The corresponding space group for the $C54$ structure is D_{2h}^{24} ($Fddd$). The Bravais lattice is face-centered orthorhombic, with primitive vectors

$$\begin{aligned} \mathbf{t}_1 &= \frac{1}{2}b\hat{j} + \frac{1}{2}c\hat{k}, \\ \mathbf{t}_2 &= \frac{1}{2}a\hat{i} + \frac{1}{2}c\hat{k}, \\ \mathbf{t}_3 &= \frac{1}{2}a\hat{i} + \frac{1}{2}b\hat{j}. \end{aligned} \quad (2)$$

The volumes of the primitive unit cells for the $C49$ and $C54$ structures are $\frac{1}{2}abc$ and $\frac{1}{4}abc$, respectively. Values⁹ for the lattice parameters and atomic position coordinates for both structures are listed in Table I.

The essential features of the $C49$ and $C54$ structures are illustrated in Fig. 1. The large and small circles represent (001) projections of the Ti and Si atoms, respectively. In Fig. 1(a) two layers of the $C49$ structure are shown. The solid (dashed) circles distinguish atoms in planes with $z = +\frac{1}{4}c$ ($-\frac{1}{4}c$). The inversion center at the

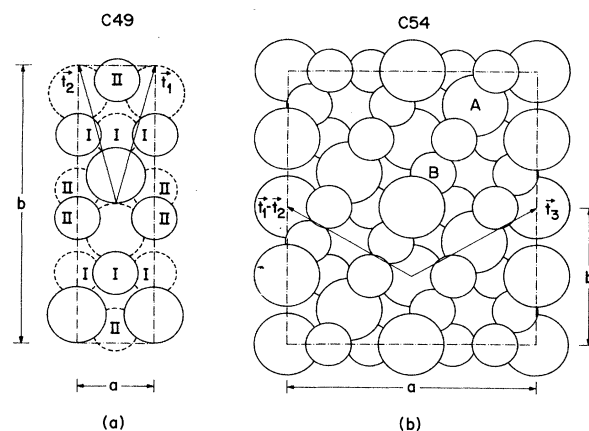


FIG. 1. Projected view of the (a) base-centered orthorhombic ($C49$) and (b) face-centered orthorhombic ($C54$) phases of TiSi_2 . The larger (smaller) circles denote Ti (Si) atom positions, respectively, as described in the text.

origin causes an interchange of the dashed and solid atoms in the figure. The two inequivalent Si atoms in the unit cell (see Table I) are labeled I and II, respectively. Each Ti atom has four nearest-neighbor Si(II) atoms [which are located in adjacent planes in Fig. 1(a)] and six more distant Si [$4\text{Si(I)} + 2\text{Si(II)}$] neighbors. Values of near-neighbor distances are summarized in Table II.

An analogous projection of the $C54$ structure is shown in Fig. 1(b). Here, three atom layers at heights $z = 0, \frac{1}{4}c$, and $\frac{1}{2}c$ are drawn, while a fourth layer is omitted for clarity. The near-neighbor coordination at the Ti and Si sites is most easily seen by considering the sites labeled A and B in the $z = \frac{1}{4}c$ plane. The Ti (or A) site has four nearest-neighbor Si atoms arranged in a distorted tetrahedral geometry. A similar environment is found at the Si (or B) site, except that two of the neighbors are Ti.

The primitive reciprocal-lattice vectors for the $C49$

TABLE II. Near-neighbor coordination at the Ti and Si sites in the orthorhombic $C49$ and $C54$ structures.

Atom	$C49$			$C54$		
	No.	Type	d (Å)	No.	Type	d (Å)
Ti	4	Si(II)	2.64	4	Si	2.54
	2	Si(I)	2.70	2	Si	2.75
	2	Si(I)	2.75	4	Si	2.76
	2	Si(II)	2.80	4	Ti	3.20
	2	Ti	3.34			
Si(I)	4	Si(I)	2.56	2+2	Ti+Si	2.54
	2	Ti	2.70	1+1	Ti+Si	2.75
	2	Ti	2.75	2+2	Ti+Si	2.76
	2	Si(II)	3.23	4	Si	3.20
Si(II)	2	Si(II)	2.33			
	4	Ti	2.64			
	2	Ti	2.80			
	2	Si(I)	3.23			

structure are given by

$$\begin{aligned} \mathbf{b}_1 &= 2\pi[(1/a)\hat{\mathbf{i}} + (1/b)\hat{\mathbf{j}}], \\ \mathbf{b}_2 &= 2\pi[-(1/a)\hat{\mathbf{i}} + (1/b)\hat{\mathbf{j}}], \\ \mathbf{b}_3 &= 2\pi[(1/c)\hat{\mathbf{k}}]. \end{aligned} \quad (3)$$

The corresponding vectors for the C54 structure are

$$\begin{aligned} \mathbf{b}_1 &= 2\pi[-(1/a)\hat{\mathbf{i}} + (1/b)\hat{\mathbf{j}} + (1/c)\hat{\mathbf{k}}], \\ \mathbf{b}_2 &= 2\pi[(1/a)\hat{\mathbf{i}} - (1/b)\hat{\mathbf{j}} + (1/c)\hat{\mathbf{k}}], \\ \mathbf{b}_3 &= 2\pi[(1/a)\hat{\mathbf{i}} + (1/b)\hat{\mathbf{j}} - (1/c)\hat{\mathbf{k}}]. \end{aligned} \quad (4)$$

Using the values of the lattice parameters that are listed in Table I, one obtains the Brillouin zones for the C49 and C54 structures which are shown in Figs. 2(a) and 2(b), respectively.

The solid lines in Fig. 2 outline each primitive Brillouin zone, while the dashed lines indicate the $\frac{1}{8}$ of each zone that forms the irreducible wedge. Vertices that are labeled with primes are equivalent to their unprimed counterparts as a result of translational symmetry so that, for example, $E(A) = E(A')$ and $E(B) = E(B')$.

The present LAPW calculations for TiSi_2 apply a rigid-core approximation with starting potentials generated from atomic valence-electron configurations of $3d^2 4s^2$ and $3s^2 3p^2$ for Ti and Si, respectively. Exchange-correlation effects are treated with the use of the Wigner interpolation formula.¹⁰ The radii of the Ti and Si muffin-tin (MT) spheres [$R(\text{Ti}) \approx 2.61$ a.u. and $R(\text{Si}) \approx 2.17$ a.u.] have been chosen so that they are nearly touching along nearest-neighbor bond directions.

The LAPW basis size has been set using a plane-wave kinetic-energy cutoff of 10 Ry, which represents about 300–325 LAPW's per primitive cell. The corresponding cutoff for the Fourier-series expansion of the interstitial charge density and potential was chosen to include ~ 5000 plane waves. The spherical-harmonic expansion of the LAPW wave functions within the MT's included terms through $l=6$. The lattice-harmonic expansion of the nonspherical contributions to the charge density and potential within the MT's included all terms with $l \leq 4$.

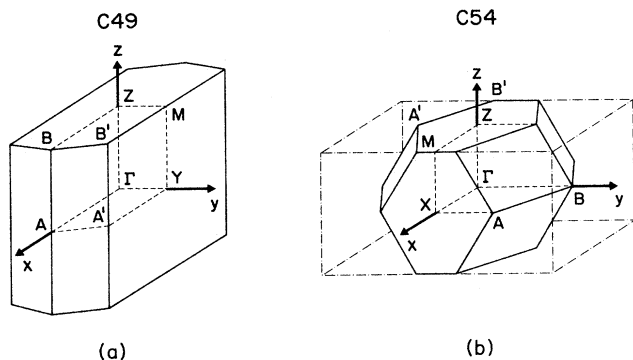


FIG. 2. Brillouin zones for the orthorhombic (a) C49 and (b) C54 polytypes of TiSi_2 .

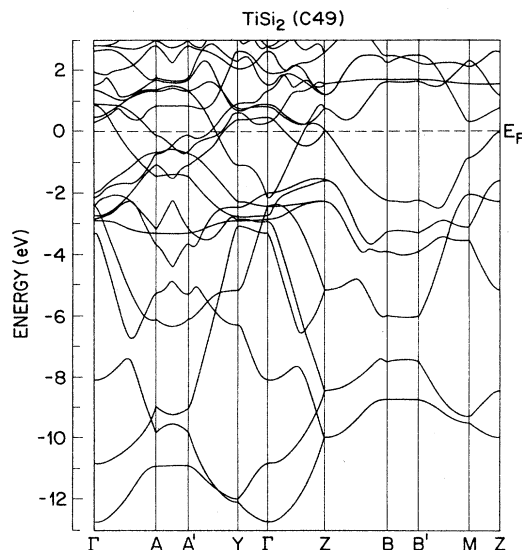


FIG. 3. LAPW energy-band results for the C49 phase of TiSi_2 .

The Brillouin-zone sampling has utilized a uniform mesh of k points in the $\frac{1}{8}$ irreducible wedge of the zone (see Fig. 2). For each structure, the mesh intervals were chosen so as to yield nearly equal increments along the three coordinate axes. A total of 32 and 27 k points were included in carrying out the self-consistent calculations for the C49 and C54 structures, respectively.

The LAPW energy-band results for the C49 and C54 phases of TiSi_2 are shown in Figs. 3 and 4, respectively. The filled bands include broad low-lying bonding combinations of Si $3s$ - $3p$ states that merge with narrower nonbonding Ti $3d$ states in the energy range 1–3 eV below E_F . The lowest unoccupied states have predom-

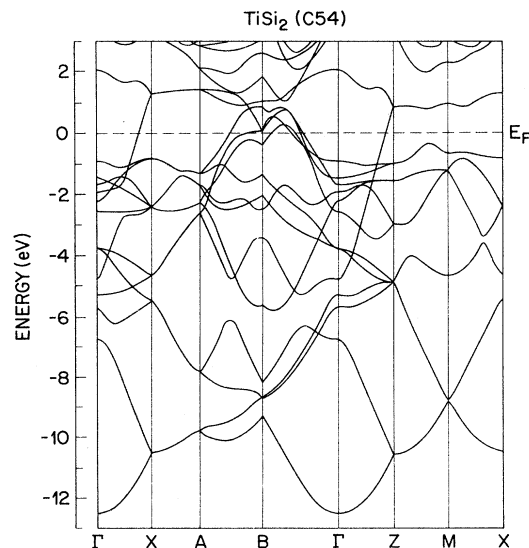


FIG. 4. LAPW energy-band results for the C54 phase of TiSi_2 .

inant Ti 3d character, so that the TiSi_2 Fermi level falls in the midst of the 10-band 3d complex.

Because of the low (D_{2h}) point symmetry of these materials, the energy-band states are, in general, singly degenerate throughout most of the Brillouin zone. Exceptions arise for states with wave vectors on the Brillouin-zone faces where a twofold ("sticking-together") degeneracy is induced by the nonsymmorphic nature of the D_{2h}^{17} and D_{2h}^{24} space groups.¹¹ Such degeneracies occur throughout the top face ($ZBB'M$) of the C49 Brillouin zone in Fig. 2(a) and along the dashed lines on the C54 Brillouin-zone faces in Fig. 2(b).

The manner in which the valence-band states evolve from low-lying Si 3s-3p bands to Ti 3d states near E_F is illustrated by the density-of-state (DOS) results in Fig. 5. These DOS curves for the C49 (C54) phase of TiSi_2 have been calculated using tetrahedral interpolation¹² based on a total of 196 (240) uniformly distributed k points in the $\frac{1}{8}$ irreducible wedge of the Brillouin zone (Fig. 2) The curves have been smoothed using a Gaussian with a full width at half maximum (FWHM) of 0.25 eV.

The total DOS is represented by the solid lines. The dashed (dotted-dashed) curves correspond to the projected DOS in which the total DOS is weighted by the integrated charge that is contained within the two Ti (four Si) MT spheres. The DOS curves for the C49 and C54 phases have similar overall features, exhibiting a generally smooth monotonic increase to maxima about 1–2 eV below E_F , then decreasing rapidly to minima near E_F .

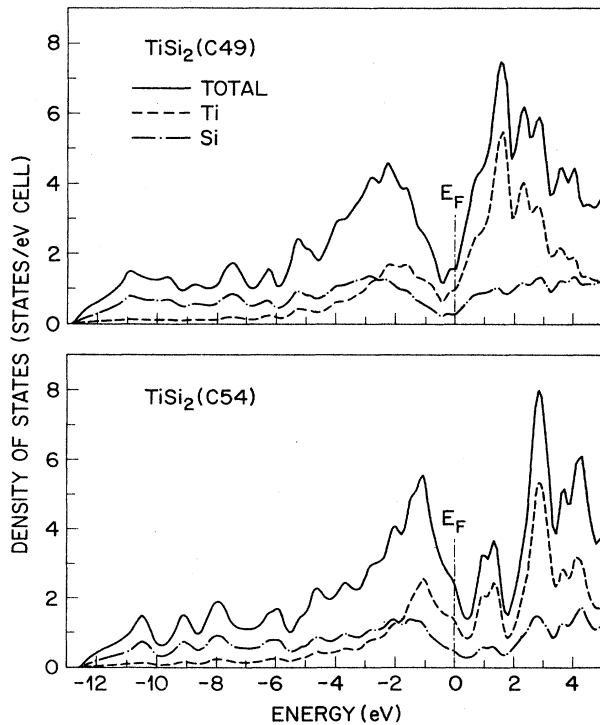


FIG. 5. Total and muffin-tin projected density-of-state curves for the C49 and C54 polytypes of TiSi_2 .

The Si-projected DOS is essentially featureless, whereas the Ti 3d component exhibits a modest peak at energies 1–3 eV below E_F and then dominates the unoccupied conduction-band states. The projected Ti 3d DOS is in reasonable agreement with ultraviolet-photoemission valence-band spectra^{6–8} which are enhanced by the large photoionization cross sections of d -type initial states.⁷

There are a total of 24 valence electrons per primitive cell for both the C49 and C54 polytypes of TiSi_2 so that, on average, a total of 12 conduction bands are occupied. Since the primitive cells contain an even number of valence electrons, both materials are compensated (i.e., they contain equal numbers of electron and hole carriers). The intersection of the TiSi_2 C49 and C54 Fermi surfaces with the central (001) Brillouin-zone plane is shown in Fig. 6. The C49 Fermi surface involves carriers in two bands: electrons in the 13th band (e_{13}) and holes in the 12th (h_{12}). Both sheets are multiply connected, allowing open orbits along the [010] direction. By comparison, the C54 Fermi surface in Fig. 6(b) consists of several closed sheets. These include a single electron pocket at Γ (e_{13}) as well as three nested hole surfaces (h_{10} – h_{12}) that are located along the [010] or ΓBM direction of the Brillouin zone. Carrier densities, broken down into partial densities for each sheet, are given in Table III.

It is interesting to consider transport properties of TiSi_2 in the context of the present band-structure results. Resistivities and Hall-effect data obtained on thin films (thickness ≈ 2000 Å) of C49 and C54 phases of TiSi_2 are summarized in Table IV. One significant difference between the metastable C49 and equilibrium C54 phases of TiSi_2 is the fact that the residual resistivity of C54 TiSi_2 is substantially lower than that for C49 TiSi_2 ($\rho_0 \approx 0.66$ versus $27 \mu\Omega \text{ cm}$). Because the low TiSi_2 resistivity is a critical characteristic in technological applications, it is important to understand the extent to which differences in the electronic band properties contribute to the ob-

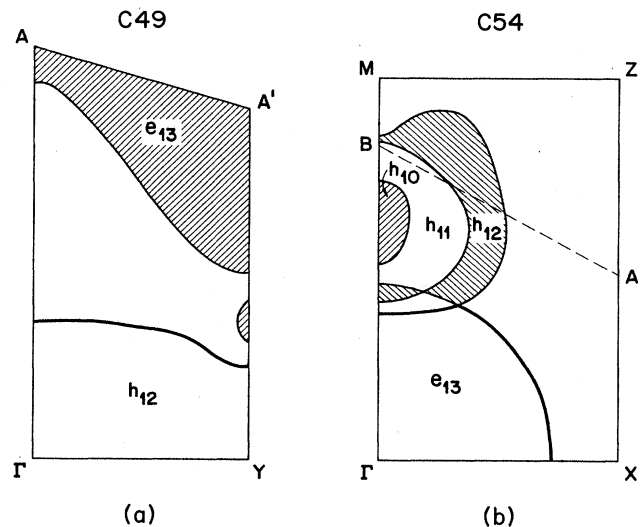


FIG. 6. Intersection of the TiSi_2 Fermi surface with a central (001) plane for the (a) C49 and (b) C54 crystal structures.

TABLE III. Summary of calculated band properties at E_F for the C49 and C54 phases of TiSi_2 .

Property	C49	C54
$N(E_F)$ (states/eV spin cell)	0.71	1.21
$n(e_{13})$ (10^{21} cm^{-3})	1.4	6.2
$n(h_{10})$ (10^{21} cm^{-3})		0.1
$n(h_{11})$ (10^{21} cm^{-3})		1.4
$n(h_{12})$ (10^{21} cm^{-3})	1.4	4.7
Ω_p (eV)	3.2	8.6
$\langle v_F^2 \rangle^{1/2}$ (10^8 cm/s)	0.49	1.00
$\langle v_x^2 \rangle^{1/2}$ (10^8 cm/s)	0.23	0.65
$\langle v_y^2 \rangle^{1/2}$ (10^8 cm/s)	0.35	0.69
$\langle v_z^2 \rangle^{1/2}$ (10^8 cm/s)	0.27	0.31

served transport properties for the two phases. This allows one to separate the intrinsic band-structure contributions from those which are extrinsic in origin.

For an isotropic system, which is the case we are considering in *polycrystalline* films of TiSi_2 , the effect of band structure on transport properties can be analyzed with the use of two calculated quantities, namely the Drude plasma energy $\Omega_p(E_F)$ and electron velocity $v(E_F)$ at the Fermi level E_F . These enter into the (scalar) resistivity in the following way:¹³

$$\rho = \frac{4\pi\hbar^2}{\Omega_p^2(E_F)} \frac{1}{\tau}, \quad (5)$$

where τ is a phenomenological scattering time. The relationship between the Drude plasma energy and the band structure is given by

$$\Omega_p^2(E_F) = \frac{8}{3}\pi e^2 \hbar^2 N(E_F) \langle v^2(E_F) \rangle, \quad (6)$$

where $N(E_F)$ is the density of states at E_F and $\langle v^2(E_F) \rangle \equiv \langle v_F^2 \rangle$ is the Fermi velocity squared, averaged over direction and over all sheets of the Fermi surface. More specifically, $\langle v_F^2 \rangle = \langle v_x^2 \rangle + \langle v_y^2 \rangle + \langle v_z^2 \rangle$, where, because of the orthorhombic symmetry of the C49 and C54 structures, the individual components $\langle v_x^2 \rangle$, $\langle v_y^2 \rangle$, and $\langle v_z^2 \rangle$ are all independent.

The calculated Drude plasma energy and Fermi velocity for C49 and C54 TiSi_2 are shown in Figs. 7 and 8, respectively. A comparison of the C49 and C54 results

TABLE IV. Resistivities and Hall coefficients for C54 and C49 phases of TiSi_2 measured at room temperature and liquid-He temperatures. The Hall effect was measured at a field of 1.5 T. For details about samples, see Ref. 4.

	T (K)	ρ ($\mu\Omega \text{ cm}$)	R_H ($10^5 \text{ cm}^3/\text{C}$)
C54	290	12.4	-4.0
	4.2	0.66	+5.5
C49	290	60	-21.2
	4.2	27	-5.9

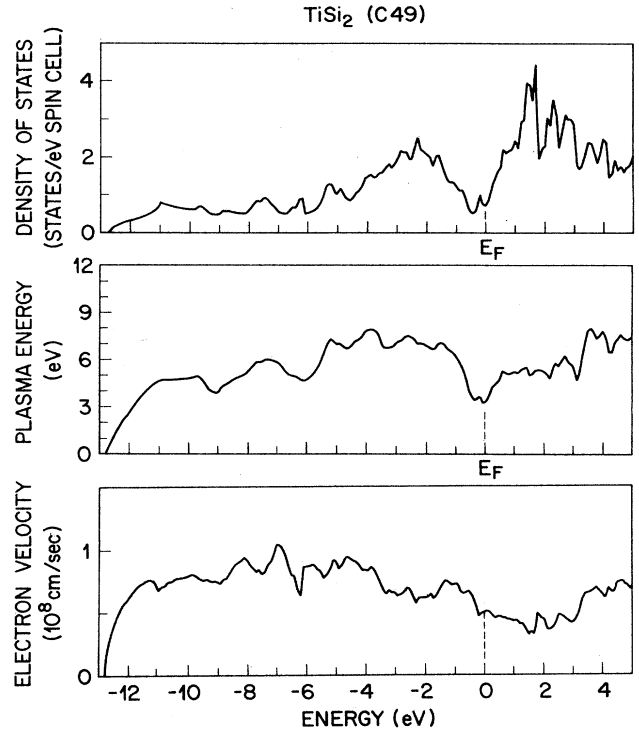


FIG. 7. Calculated density of states, Drude plasma energy, and Fermi velocity for TiSi_2 (C49).

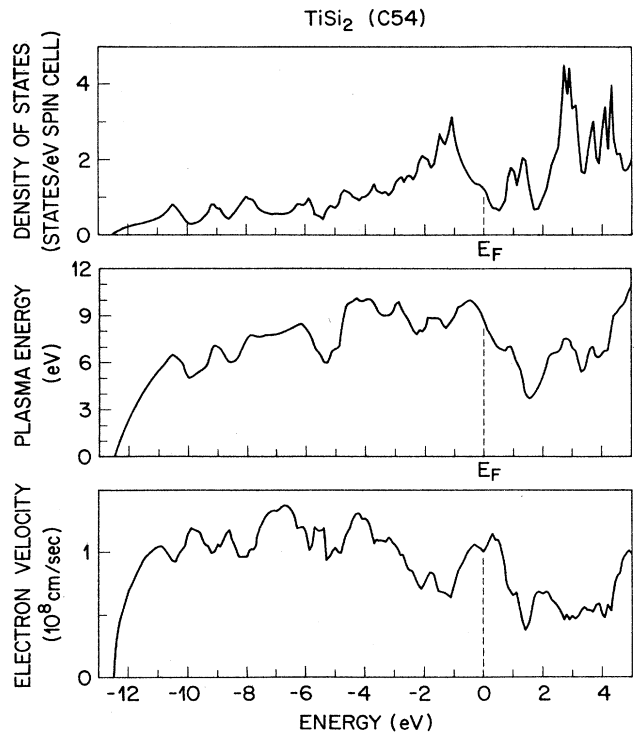


FIG. 8. Calculated density of states, Drude plasma energy, and Fermi velocity for TiSi_2 (C54).

shows that the values for the Drude plasma energy and carrier velocity are notably higher for the C54 polytype. This is also reflected by the values at E_F , which are summarized in Table III.

The calculated Drude plasma energy and Fermi velocity can be combined with the observed residual resistivity ρ_0 to determine important transport parameters such as the electron scattering length $l_c = \langle v_F^2 \rangle^{1/2} \tau$ using relation (5). Introducing the observed values of ρ_0 (see Table IV) for the C49 (27 $\mu\Omega$ cm) and C54 (0.66 $\mu\Omega$ cm) phases yields the liquid-He-temperature scattering lengths $l_c \approx 90$ Å (C49) and $l_c \approx 990$ Å (C54). Because of band-structure effects, the 40-fold difference in the residual resistivities leads to a 10-fold difference in the electron scattering lengths for the C49 and C54 phases. It seems quite likely that the heavily faulted microstructure that has been reported^{2,3} for C49 TiSi₂ films is responsible for the relatively short scattering length and high resistivity of this material.

The Hall-effect data in Table IV illustrate an important point sometimes overlooked, namely that for the case of a complex band structure such as that of TiSi₂ the low-field Hall effect is not sufficiently tractable to be of much help in the analysis of the transport data and, in fact, if applied indiscriminately, can lead to erroneous results. The strong temperature dependence of R_H seen in Table IV (R_H even reverses sign for the C54 phase) should be a warning that things are far from simple. But if one were to ignore this and attempt to make a crude estimate of carrier densities from $(R_H e c)^{-1}$, the numbers would be totally unrealistic, i.e., $\sim 5 \times 10^{22}$ carriers/cm³ for C49 TiSi₂ and $\sim 1 \times 10^{23}$ carriers/cm³ for C54 TiSi₂, values which are more than an order of magnitude larger than the calculated densities in Table III. The problem is that this single-band model ignores the important fact that TiSi₂ is *compensated*, resulting in partial cancellation of Hall fields from electrons and holes. Multiband models¹⁴ seldom provide a satisfactory solution since they intro-

duce a proliferation of empirical parameters. A more sophisticated (and correct) approach could be made using band-structure results, but little is gained thereby. It is better to apply the band results directly to the resistivity data, as we have done above.

Finally, we comment on the implications of crystal anisotropy on the transport properties of the C49 and C54 phases of TiSi₂. It is worth noting that the carrier-velocity components are reasonably isotropic for the C49 phase, despite the layered arrangement of Ti atoms in this structure. On the other hand, $\langle v_z^2 \rangle^{1/2}$ is significantly smaller than $\langle v_x^2 \rangle^{1/2}$ and $\langle v_y^2 \rangle^{1/2}$ over most of the valence-band energy range, including E_F , for the C54 polytype. This anisotropy, which is not immediately evident from the C54 crystal structure or band profiles, may have important implications concerning the transport properties of TiSi₂ thin films. In fact, resistivity data¹⁵ have become available quite recently for single-crystal C54 TiSi₂. Equation (5) does not apply in this anisotropic case, and we should use instead the more general expression, $\rho_{ii}^{-1} = 2e^2 \tau N(E_F) \langle v_i^2(E_F) \rangle$, where $i = x, y, z$. Using the mean squares of the Fermi velocities from Table III, one obtains the theoretical resistivity anisotropy expressed as a ratio: $\rho_{xx} : \rho_{yy} : \rho_{zz} = 1.00 : 0.89 : 4.41$. The observed room-temperature resistivity anisotropy ratio 1.00:0.93:1.06 correlates in "sense" but appears to be considerably weaker, for reasons that are not evident. (Even more curious is the fact that the sense of the anisotropy reverses at liquid-He temperatures, i.e. a residual resistivity ratio of 1.00:1.15:0.75.)

To summarize, we have calculated the electronic band structure and properties of the metastable C49 and equilibrium C54 phases of TiSi₂. The results exhibit many qualitative similarities, including a density-of-states minimum within the Ti 3d manifold near E_F . The calculated electron-scattering lengths in the low-resistivity TiSi₂ C54 phase ($l_c \approx 1000$ Å) are an order of magnitude longer than those estimated for the C49 polytype.

¹S. P. Murarka, *J. Vac. Sci. Technol.* **17**, 775 (1980).

²R. Beyers and S. Sinclair, *J. Appl. Phys.* **57**, 5240 (1985).

³H. J. W. van Houtum and I. J. M. M. Raaijmakers, *Mater. Res. Soc. Symp. Proc.* **54**, 37 (1986).

⁴J. C. Hensel, J. M. Vandenberg, L. F. Mattheiss, F. C. Unterwald, and A. Maury, *Mater. Res. Soc. Symp. Proc.* **77**, 737 (1987); J. C. Hensel, J. M. Vandenberg, F. C. Unterwald, and A. Maury, *Appl. Phys. Lett.* **51**, 1100 (1987).

⁵L. F. Mattheiss and D. R. Hamann, *Phys. Rev. B* **33**, 823 (1986).

⁶A. Franciosi and J. H. Weaver, *Physica B+C* **117&118B**, 846 (1983).

⁷J. H. Weaver, A. Franciosi, and V. L. Moruzzi, *Phys. Rev. B* **29**, 3293 (1984).

⁸G. Petö, E. Zsoldos, L. Guzzi, and Z. Schay, *Solid State Com-*

mun. **57**, 817 (1986).

⁹W. B. Pearson, *A Handbook of Lattice Spacings and Structures of Metals and Alloys* (Pergamon, New York, 1967), Vol. 2.

¹⁰E. Wigner, *Phys. Rev.* **46**, 1002 (1934).

¹¹A. P. Cracknell, B. L. Davies, S. C. Miller, and W. F. Love, *Kronecker Product Tables* (Plenum, New York, 1979), Vol. I.

¹²O. Jepsen and O. K. Andersen, *Solid State Commun.* **9**, 1763 (1971); G. Lehmann and M. Taut, *Phys. Status Solid B* **54**, 469 (1972).

¹³L. F. Mattheiss and L. R. Testardi, *Phys. Rev. B* **20**, 2196 (1979).

¹⁴J. C. Hensel, *Mater. Res. Soc. Symp. Proc.* **54**, 499 (1986).

¹⁵O. Thomas, R. Madar, J. P. Senateur, and O. Laborde, *J. Less-Common Met.* **136**, 175 (1987).